2021-11-24

Dynamic stability of CNTs-reinforced non-uniform composite beams under axial excitation loading

Yuan, W-B

10.1016/j.commatsci.2021.111054
Computational Materials Science
Elsevier

Computational Materials Science
https://doi.org/10.1016/j.commatsci.2021.111054
Accepted 12 November 2021

Dynamic stability of CNTs-reinforced non-uniform composite beams under axial excitation loading

Wei-bin Yuan[1], Long-Yuan Li[2*], Sung-Hwan Jang[3]

[1] College of Architecture and Civil Engineering, Zhejiang University of Technology, Hangzhou 310023, China (yuanwb@zjut.edu.cn)
[2] School of Engineering, Computing and Mathematics, University of Plymouth, Plymouth, Devon PL4 8AA, UK (long-yuan.li@plymouth.ac.uk)
[3] School of Engineering, Hanyang University ERICA, Ansan, Gyeonggi-do 15588, South Korea (sj2527@hanyang.ac.kr)
* Corresponding author

Abstract - This paper presents an analytical study on the dynamic stability of carbon nanotubes (CNTs) reinforced functionally graded composite beams when subjected to axial excitation loading. The composite beams are functionally graded using a I-type CNTs reinforcement. The section properties of the non-uniform functionally graded composite beams are assessed using Halpin–Tsai model. The analysis of dynamic stability of the composite beams is performed by using Bolotin's method. Analytical expressions of determining free vibration frequency, critical buckling load, and excitation frequency of the non-uniform functionally graded composite beams are derived, in which both the shear deformation and rotary inertia effects are considered. The study demonstrates that the dynamic stability of the beam can be improved significantly when it is functionally graded using the I-type CNTs reinforcement.

Keywords: Carbon nanotubes; Composite beams; Functionally graded; Excitation loading; Dynamic instability.

1. Introduction

Carbon nanotubes (CNTs) have received tremendous attention since they were discovered in 1991 and become popular in recent years. CNTs have excellent mechanical, thermal and electrical properties [1,2] and have great potential for applications in many scientific and technological fields, especially for use as composite fillers in polymers to improve the mechanical, thermal, and electrical properties of resulting composites. Examples include CNTs-smart sensors, CTNs-functionally graded (FG) composites, CNTs strengthened structural composites [3], etc. An excellent literature review has been provided by Coleman et al. [4] on the mechanical properties of CNTs-polymer composites.

In recent years, CNTs have been applied to structures to provide structural health monitoring functions. In order to effectively and efficiently use CNTs in a structure, often, CTNs are first mixed with polymer to produce a CNTs-polymer composite, and then the composite is incorporated into the structure to monitor the overall structural behaviors. To implement the functions of CNTs, one has to understand not only the properties of CNTs-filled composite but also the interactions between the CNTs-filled composite and its monitored structure. Extensive research works have been carried out since CNTs were discovered. For instance, Chakraborty

et al. [5] developed a beam finite element for the analysis of FG materials. Li [6] proposed a unified approach for analyzing the static and dynamic behaviors of FG beams. Şimşek [7] used Ritz method to analyze the static behavior of FG beams subjected to uniformly distributed loading. Huang and Li [8] presented the free vibration analysis of axially FG beams with non-uniform cross-section. Alshorbagy et al. [9] analyzed the free vibration problem of FG beams by using finite element method. Lezgy-Nazargah et al. [10] presented a refined high-order theory for bending and vibration analyses of laminated composite beams. Rokni et al. [11,12] demonstrated the improvement of dynamic properties of composite beams reinforced by CNTs. Ansari et al. [13] performed the nonlinear forced vibration analysis of FG composite beams reinforced by CNTs. Filippi et al. [14] provided a comparable study on the static analysis of FG beams by using different theories and finite element method. Lezgy-Nazargah [15] and El-Ashmawy et al. [16] investigated the thermo-mechanical behaviors of FG beams. Shafiei and Kazemi [17] presented the buckling analysis of bi-dimensional FG porous tapered nano- and micro-scale beams. Yang et al. [18] conducted the bending, buckling and vibration analyses of bi-directional FG nano-scale beams. Lal and Markad [19] studied the deflection and stress behavior of multi-walled CNTs reinforced laminated composite beams. Ranjbar and Feli [20] conducted the low velocity impact analysis of axially FG CNTs-reinforced beams. Zheng et al. [21] reported the size dependent nonlinear free vibration of axially FG tapered micro-beams using finite element method. Aubad et al. [22] presented the modal analysis and transient response of axially FG beams using finite element method. Sahmani and Safaei [23], Tang et al. [24], Heidari and Arvin [25] investigated the nonlinear free vibrations of FG CNTs-reinforced beams. Chen et al. [26] presented the static and dynamic analyses of post-buckling of bi-directional FG micro-beams. Lal and Markad [27] presented the thermo-mechanical post-buckling analysis of CNTs-reinforced laminated beams on elastic foundation. Sahmani and Safaei [28] examined the influence of homogenization models on the size-dependent nonlinear bending and post-buckling of bi-directional FG micro- and nano-beams. Bourada et al. [29] performed the stability and dynamic analyses of CNTs-reinforced concrete beams on elastic foundation. El-Ashmawy and Xu [30] presented a longitudinal modeling and properties tailoring of FG CNTs-reinforced composite beams. Yang et al. [31] investigated the nonlinear flexural behavior of temperature dependent FG CNTs-reinforced laminated beams with negative Poisson's ratio resting on the Pasternak foundation. Khaniki and Ghayesh [32] examined the dynamic characteristics of axially FG CNT-strengthened deformable beams. Hou et al. [33] reported a computational model for the static analysis of axially FG micro-cylindrical imperfect beam. Shariati et al. [34] presented a study on the stability and dynamics of viscoelastic moving Rayleigh beams with an asymmetrical distribution of material parameters. Apart from the work on CNTs-reinforced FG composite beams mentioned above, studies were also reported on the vibration and buckling of graphene nanoplatelet-reinforced composite disks and cylindrical shells [35,36].

The aforementioned literature survey shows that there have been extensive studies on the CNTs-reinforced FG composite beams. The research covers the bending, buckling, free vibration and dynamic response analyses of the beams with various different FG distributions of CNTs, either in the longitudinal direction or on the cross-section of the beams. However, limited work exists on the interaction of the buckling and vibration of CNTs-reinforced FG composite beams when subjected to axial excitation loading. In this paper, a study is carried out on the dynamic instability of CNTs-reinforced FG composite beams when subjected to axial excitation loading. Unlike the existing studies in which the V-, O-, X- and Λ-types of FG distributions of CNTs on the cross-section of the beam were used [37,38], the present study uses an I-type FG distribution, which comes from the idea of the traditional I-section steel

beams, which can provide better performance in terms of both the bending and shear behaviors. By assuming the instability modes, the kinetic energy and strain energy of the composite beams and the loss of the potential of the axially compressive load are evaluated, from which the generalized equation of motion of the CNTs-reinforced FG composite beams is derived. The analysis of the dynamic instability of the composite beams is performed by using Bolotin method [39,40,41,42,43]. Numerical examples are provided for illustrating the dynamic instability behavior of the CNTs-reinforced FG composite beams when subjected to axial excitation loading. The obtained results elucidate how the composite beam can be reinforced non-uniformly by using CNTs in order to improve its dynamic stability.

2. Mechanical properties of CNTs-reinforced composite beams

Consider a composite beam made from polymer matrix material reinforced with CNTs. In literature various different FG distributions of CNTs such as V-, O-, X- and Λ-types on the cross-section of the beam have been proposed [37,38]. However, for a structural element, the beam with an I-section would be desirable because of its effectiveness in terms of the bending, which is resisted mainly by the two flanges, and shear, which is resisted largely by the web of the I-section beam. In order to achieve the I-section-type properties in a composite beam with rectangular cross-section, the "I"-type FG distribution of CNTs (see Fig.1) is used in the present study. The purpose of using such an I-type distribution of CNTs is for improving both the bending and shear performance of the composite beam. More importantly, by adjusting the volume fractions of CNTs used in the two outer layers and core layer of the beam one can optimize the properties of the FG composite beams. Assume the volume fraction of CNTs is V_{c1} in the top and bottom layers and V_{c2} in the middle part of the beam, respectively. The overall volume fraction of CNTs in the beam thus can be expressed as follows,

$$V_c = \frac{2tbV_{c1}+(h-2t)bV_{c2}}{hb} \tag{1}$$

where V_c is the overall volume fraction of CNTs in the beam, t is the thickness of the top or bottom layer of the beam, b is the width of the beam, and h is the depth of the beam. V_{c1} and V_{c2} can be adjusted in terms of required functions. According to Halpin–Tsai model [3,44], the Young's modulus, Poisson's ratio, shear modulus and density of the CNTs-reinforced composite beams are the function of y-coordinate and can be expressed as follows,

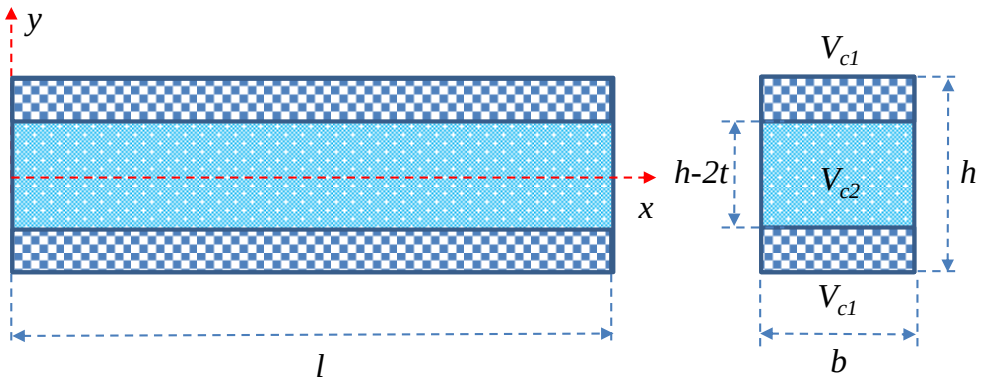

Fig.1. Length and cross-section dimensions of CNTs-reinforced composite beam.

For zone: y>(h/2–t) or y<-(h/2–t)

$$E_{e1} = \frac{3}{8}\left(\frac{1+2\lambda\eta_L V_{c1}}{1-\eta_L V_{c1}}\right) E_m + \frac{5}{8}\left(\frac{1+2\eta_T V_{c1}}{1-\eta_T V_{c1}}\right) E_m \quad (2)$$

$$\nu_{e1} = V_{c1}\nu_c + (1 - V_{c1})\nu_m \quad (3)$$

$$G_{e1} = \frac{E_{e1}}{2(1+\nu_{e1})} \quad (4)$$

$$\rho_{e1} = V_{c1}\rho_c + (1 - V_{c1})\rho_m \quad (5)$$

For zone: -(h/2-t)⩽y⩽(h/2-t)

$$E_{e2} = \frac{3}{8}\left(\frac{1+2\lambda\eta_L V_{c2}}{1-\eta_L V_{c2}}\right) E_m + \frac{5}{8}\left(\frac{1+2\eta_T V_{c2}}{1-\eta_T V_{c2}}\right) E_m \quad (6)$$

$$\nu_{e2} = V_{c2}\nu_c + (1 - V_{c2})\nu_m \quad (7)$$

$$G_{e2} = \frac{E_{e2}}{2(1+\nu_{e2})} \quad (8)$$

$$\rho_{e2} = V_{c2}\rho_c + (1 - V_{c2})\rho_m \quad (9)$$

in which,

$$\eta_L = \frac{E_c - E_m}{E_c + 2\lambda E_m} \quad (10)$$

$$\eta_T = \frac{E_c - E_m}{E_c + 2E_m} \quad (11)$$

where E_{e1}, ν_{e1}, G_{e1} and ρ_{e1} are the effective Young's modulus, effective Poisson's ratio, effective shear modulus and effective density in the top and bottom layers of the beam, E_{e2}, ν_{e2}, G_{e2} and ρ_{e2} are the effective Young's modulus, effective Poisson's ratio, effective shear modulus and effective density in the middle part of the beam, E_c, ν_c and ρ_c are the Young's modulus, Poisson's ratio and density of the CNTs, E_m, ν_m and ρ_m are the Young's modulus, Poisson's ratio and density of the polymer matrix material, and λ is the aspect ratio of CNTs fibers.

3. Vibration, buckling and dynamic instability analyses of CNTs-reinforced composite beams

Assume that the CNTs-reinforced composite beam shown in Fig.1 can be treated as the Timoshenko beam [25,45], in which two independent displacements are the transverse displacement w(x,t) and angle of rotation of the cross-section ϕ(x,t). According to the Timoshenko beam theory where both the shear deformation and rotary inertia effects are considered, the kinetic energy of the composite beam at any time t can be expressed as follows,

$$T(t) = \frac{1}{2}(\rho A)_{eq}\int_o^l \left(\frac{\partial w}{\partial t}\right)^2 dx + \frac{1}{2}(\rho I)_{eq}\int_o^l \left(\frac{\partial \phi}{\partial t}\right)^2 dx \quad (12)$$

where T(t) is the kinetic energy of the beam, l is the beam length, $(\rho A)_{eq}$ and $(\rho I)_{eq}$ are the mass and moment of inertia per-unit length, respectively, which can be calculated as follows,

$$(\rho A)_{eq} = 2\rho_{e1} bt + \rho_{e2} b(h - 2t) \quad (13)$$

$$(\rho I)_{eq} = 2\rho_{e1} bt\left(\frac{h-t}{2}\right)^2 + 2\rho_{e1}\frac{bt^3}{12} + \rho_{e2}\frac{b(h-2t)^3}{12} \quad (14)$$

The strain energy of the composite beam at any time t can be expressed as follows,

$$U(t) = \frac{1}{2}(EI)_{eq}\int_o^l \left(\frac{\partial \phi}{\partial x}\right)^2 dx + \frac{k_s}{2}(GA)_{eq}\int_o^l \left(\frac{\partial w}{\partial x} - \phi\right)^2 dx \tag{15}$$

where U(t) is the strain energy of the beam, k_s =1.2 is the shear factor, $(EI)_{eq}$ and $(GA)_{eq}$ are the flexural and shear rigidities of the beam, respectively, which can be calculated as follows,

$$(EI)_{eq} = 2E_{e1}bt\left(\frac{h-t}{2}\right)^2 + 2E_{e1}\frac{bt^3}{12} + E_{e2}\frac{b(h-2t)^3}{12} \tag{16}$$

$$\begin{aligned}(GA)_{eq} &= 3b\int_o^{\frac{h}{2}-t} G_{e2}\left[1-\left(\frac{2y}{h}\right)^2\right]dy + 3b\int_{\frac{h}{2}-t}^{\frac{h}{2}} G_{e1}\left[1-\left(\frac{2y}{h}\right)^2\right]dy \\ &= bh\left[G_{e1} - \frac{3}{2}\left(1-\frac{2t}{h}\right)(G_{e1}-G_{e2}) + \frac{1}{2}\left(1-\frac{2t}{h}\right)^3(G_{e1}-G_{e2})\right]\end{aligned} \tag{17}$$

In Eq.(17) the shear rigidity is calculated based on the parabolic distribution assumption of shear strain along the thickness direction. The loss of potential of the externally applied axial load P(t) at any time t can be expressed as follows,

$$W(t) = \frac{1}{2}P(t)\int_o^l \left(\frac{\partial w}{\partial x}\right)^2 dx \tag{18}$$

where P(t) is the externally applied axial load. For a simply supported beam, the displacement functions w(x,t) and ϕ(x,t) satisfying the boundary conditions can be approximately assumed as follows,

$$w(x,t) = C_1(t)\sin\frac{\pi x}{l} \tag{19}$$

$$\phi(x,t) = C_2(t)\cos\frac{\pi x}{l} \tag{20}$$

where $C_1(t)$ and $C_2(t)$ are the functions of time which are to be determined lately. Substituting Eqs.(19) and (20) into Eqs.(12), (15) and (18), it yields,

$$T(t) = \frac{l}{4}(\rho A)_{eq}\dot{C}_1^2 + \frac{l}{4}(\rho I)_{eq}\dot{C}_2^2 \tag{21}$$

$$U(t) = \frac{l}{4}(EI)_{eq}\left(\frac{\pi}{l}\right)^2 C_2^2 + \frac{k_s l}{4}(GA)_{eq}\left(\frac{\pi}{l}C_1 - C_2\right)^2 \tag{22}$$

$$W(t) = \frac{l}{4}P(t)\left(\frac{\pi}{l}\right)^2 C_1^2 \tag{23}$$

By applying Hamilton's principle, the following equations of motion of the beam can be obtained,

$$(\rho A)_{eq}\ddot{C}_1 + \frac{\pi}{l}k_s(GA)_{eq}\left(\frac{\pi}{l}C_1 - C_2\right) - P(t)\left(\frac{\pi}{l}\right)^2 C_1 = 0 \tag{24}$$

$$(\rho I)_{eq}\ddot{C}_2 + (EI)_{eq}\left(\frac{\pi}{l}\right)^2 C_2 - k_s(GA)_{eq}\left(\frac{\pi}{l}C_1 - C_2\right) = 0 \tag{25}$$

It is obvious that if there is no external load, that is P(t)=0, Eqs.(24) and (25) reduce to the free vibration equations of two degrees of freedom, from which the natural frequencies of the beam can be obtained by solving the following eigenvalue equations,

$$\begin{Vmatrix} -(\rho A)_{eq}\omega^2 + k_s(GA)_{eq}\left(\frac{\pi}{l}\right)^2 & -k_s(GA)_{eq}\left(\frac{\pi}{l}\right) \\ -k_s(GA)_{eq}\left(\frac{\pi}{l}\right) & -(\rho I)_{eq}\omega^2 + (EI)_{eq}\left(\frac{\pi}{l}\right)^2 + k_s(GA)_{eq} \end{Vmatrix} = 0 \quad (26)$$

where ω is the natural frequency of the transverse vibration of the beam. The smaller frequency of Eq.(26) is given as follows,

$$\omega^2 = \frac{1}{2}\left[\left(\frac{k_s(GA)_{eq}}{(\rho A)_{eq}}\left(\frac{\pi}{l}\right)^2 + \frac{(EI)_{eq}}{(\rho I)_{eq}}\left(\frac{\pi}{l}\right)^2 + \frac{k_s(GA)_{eq}}{(\rho I)_{eq}}\right) - \sqrt{\left(\frac{k_s(GA)_{eq}}{(\rho A)_{eq}}\left(\frac{\pi}{l}\right)^2 + \frac{(EI)_{eq}}{(\rho I)_{eq}}\left(\frac{\pi}{l}\right)^2 + \frac{k_s(GA)_{eq}}{(\rho I)_{eq}}\right)^2 - \frac{4k_s(GA)_{eq}(EI)_{eq}}{(\rho A)_{eq}(\rho I)_{eq}}\left(\frac{\pi}{l}\right)^4}\right] \quad (27)$$

It is observable from Eq.(27) that if the shear deformation is ignored, that is $(GA)_{eq} \to \infty$, the frequency given by Eq.(27) reduces to the fundamental frequency of the simply supported Euler-Bernoulli beam.

If the external load is applied statically, then Eqs.(24) and (25) reduce to the static stability equations of the beam at bifurcation equilibrium state, from which the critical buckling load can be obtained by solving the following eigenvalue equation,

$$\begin{Vmatrix} k_s(GA)_{eq}\left(\frac{\pi}{l}\right)^2 - P_{cr}\left(\frac{\pi}{l}\right)^2 & -k_s(GA)_{eq}\left(\frac{\pi}{l}\right) \\ -k_s(GA)_{eq}\left(\frac{\pi}{l}\right) & (EI)_{eq}\left(\frac{\pi}{l}\right)^2 + k_s(GA)_{eq} \end{Vmatrix} = 0 \quad (28)$$

where P_{cr} is the critical buckling load of the beam and can be expressed as follows,

$$P_{cr} = \frac{\pi^2(EI)_{eq}}{l^2}\frac{k_s(GA)_{eq}l^2}{k_s(GA)_{eq}l^2 + \pi^2(EI)_{eq}} \quad (29)$$

Again, it can be seen from Eq.(29) that if the shear deformation is ignored, i.e. $(GA)_{eq} \to \infty$, the critical buckling load given by Eq.(29) reduces to the classical Euler buckling load.

If the external load is a periodic one, that is $P(t) = \alpha\cos(\Omega t)$, where α is the amplitude and Ω is the excitation frequency of the dynamic load, the solution of Eq.(24) and (25) can be expressed as follows,

$$\begin{Bmatrix} C_1(t) \\ C_2(t) \end{Bmatrix} = \sum_{k=1,2,3\ldots}\left(\begin{Bmatrix} a_{1k} \\ a_{2k} \end{Bmatrix}\sin\frac{k\Omega t}{2} + \begin{Bmatrix} b_{1k} \\ b_{2k} \end{Bmatrix}\cos\frac{k\Omega t}{2}\right) \quad (30)$$

where a_{1k}, a_{2k}, b_{1k}, and b_{2k} (k=1,2,3,…) are the coefficients of the solution. It is known that [39-43], for a given amplitude of the load the dynamic instability regions of the dynamic system described by Eqs.(24) and (25) can be determined by examining the periodic solutions with the periods of $T=2\pi/\Omega$ and $2T=4\pi/\Omega$. The solution with the period of 2T is of particular importance, representing the primary instability region of the system, which can be expressed using the form of trigonometric series given by Eq.(30). Substituting Eq.(30) into (24) and (25) and letting the coefficients of the series associated with $\sin(\Omega t/2)$ and $\cos(\Omega t/2)$ be zero, it yields,

$$\begin{Vmatrix} k_s(GA)_{eq}\left(\frac{\pi}{l}\right)^2 \pm \frac{\alpha}{2}\left(\frac{\pi}{l}\right)^2 - (\rho A)_{eq}\frac{\Omega^2}{4} & -k_s(GA)_{eq}\left(\frac{\pi}{l}\right) \\ -k_s(GA)_{eq}\left(\frac{\pi}{l}\right) & (EI)_{eq}\left(\frac{\pi}{l}\right)^2 + k_s(GA)_{eq} - (\rho I)_{eq}\frac{\Omega^2}{4} \end{Vmatrix} = 0 \quad (31)$$

Eq.(31) leads to the following expression for the excitation frequency of the dynamic load,

$$\frac{\Omega^2}{4}=\frac{1}{2}\left(\frac{\pi}{l}\right)^2\left[\left(\frac{k_S(GA)_{eq}\pm\frac{\alpha}{2}}{(\rho A)_{eq}}+\frac{(EI)_{eq}}{(\rho I)_{eq}}+\frac{k_S(GA)_{eq}l^2}{\pi^2(\rho I)_{eq}}\right)-\sqrt{\left(\frac{k_S(GA)_{eq}\pm\frac{\alpha}{2}}{(\rho A)_{eq}}+\frac{(EI)_{eq}}{(\rho I)_{eq}}+\frac{k_S(GA)_{eq}l^2}{\pi^2(\rho I)_{eq}}\right)^2-\frac{4(k_S(GA)_{eq}\pm\frac{\alpha}{2})(EI)_{eq}\pm2\alpha k_S(GA)_{eq}\left(\frac{l}{\pi}\right)^2}{(\rho A)_{eq}(\rho I)_{eq}}}\right] \quad (32)$$

In terms of the format Eq.(32) is similar to Eq.(27), but they have two differences. One is the frequency. The frequency ω in Eq.(27) is the natural frequency of the beam; whereas the frequency Ω in Eq.(32) represents the excitation frequency of the dynamic load. The other is the stiffness. The stiffness in Eq.(31) is modified by the externally applied axial dynamic load. Note that there is a symbol "±" in Eqs.(31) and (32) representing two separate operations. For "+" operation the stiffness is strengthened; whereas for "-" operation the stiffness is weakened. Thus, for a given value of α, one can calculate two frequencies of Ω, one corresponds to "+" operation and the other is related to "-" operation, which give the boundary of dynamic instability region of the beam when it is subjected to an axial excitation loading. The dynamic instability zone predicted by Eq.(32) can be applied to any Timoshenko beams. However, since the particular definitions of the section properties given by Eqs.(13), (14), (16) and (17), Eq.(32) is more general and can be used to examine the effect of CTNs FG dispersion on the dynamic instability of the reinforced composite beams.

4. Numerical examples

As the numerical examples, here a CNTs-reinforced-polymer composite beam is analyzed. The dimensions of the composite beam analyzed are: beam width b=20 mm, beam depth h=60 mm, and beam top/bottom layer thickness t=6 mm. The beam length is taken from l=3h to l=10h for the free vibration and buckling analyses, and l=4h and l=8h for the dynamic instability analyses. The mechanical properties of CNTs and polymer materials used are given in Table 1, which are taken from literature [12]. For each type of analyses, four different cases are considered. Case 1 is the non-reinforced-polymer beam ($V_{c1}=V_{c2}=V_c=0$) which serves as the reference beam for the purpose of comparison; Case 2 is the uniformly reinforced CNTs-polymer composite beam (that is $V_{c1}=V_{c2}=V_c$); Case 3 is the I-type CNTs-reinforced FG composite beam with $V_{c1}=5V_{c2}$; Case 4 is also the I-shape CNTs-reinforced FG composite beam with $V_{c1}=10V_{c2}$. Note that since the total CNTs used in the beam for cases 2, 3 and 4 are identical, any increase in V_{c1} means that there would be a decrease in V_{c2}, as determined by Eq.(1), provided that V_{c2} is not less than the threshold volume fraction of the inclusions [46,47]. Physically, the larger of V_{c1} (or the smaller of V_{c2}) implies that the equivalent beam has larger width of flanges or thinner thickness of the web.

Table 1 Mechanical properties of polymer and CNTs

Parameter	**Polymer matrix**	**CNTs**
Young's modulus (GPa)	E_m = 1.90	E_c = 900
Poisson's ratio	ν_m = 0.340	ν_c = 0.280
Density (kg/m^3)	ρ_m =1050	ρ_c = 2100
Aspect ratio	-	50

Fig.2 shows the variation of the natural frequency of the composite beams with the beam length for beams with two different overall volume fractions of CNTs, V_c=1.5% and V_c=5.0%, respectively. The results are obtained from the calculation of Eq.(27). It can be seen from the figure that the frequencies of the three composite beams are much greater than that of the reference beam, indicating that the use of small quantity of CNTs can significantly improve the vibration performance of the composite beams. The frequencies of the two I-shape CNTs-reinforced FG composite beams are found to be higher than that of the uniformly reinforced CNTs-polymer composite beam, indicating that the use of I-shape FG distribution is more effective. The frequencies of the two I-shape CNTs-reinforced FG composite beams however do not have substantial difference, indicating that there is a limitation by increasing the volume fraction of CNTs in the two outer layers of the beams because of the required balance between the shear and flexural rigidities. Also, it can be observed by comparing the frequencies shown in Fig.2a and Fig.2b that, the more the CNTs used in the beam, the more increase in frequency can be achieved, which is also expected.

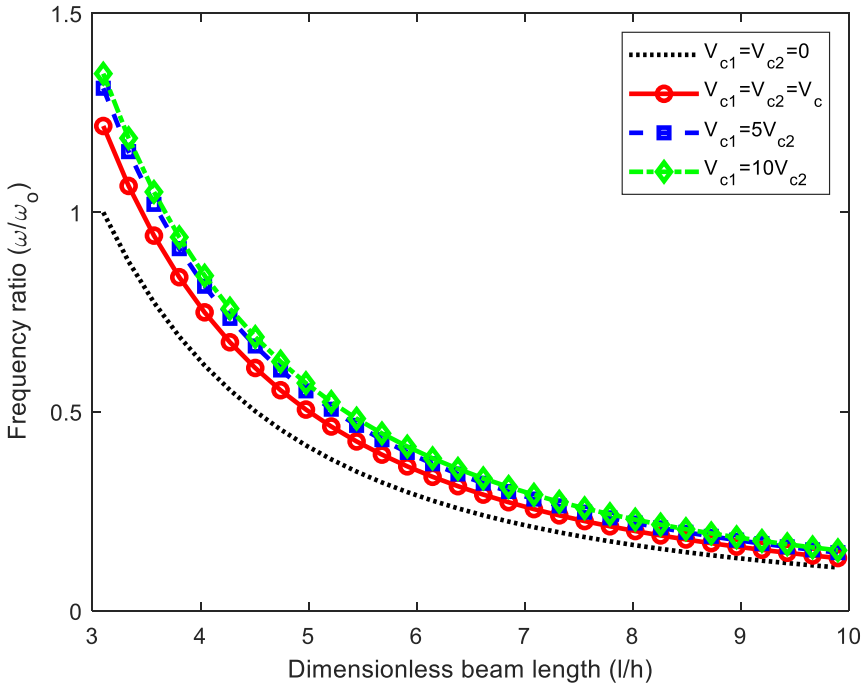

(a)

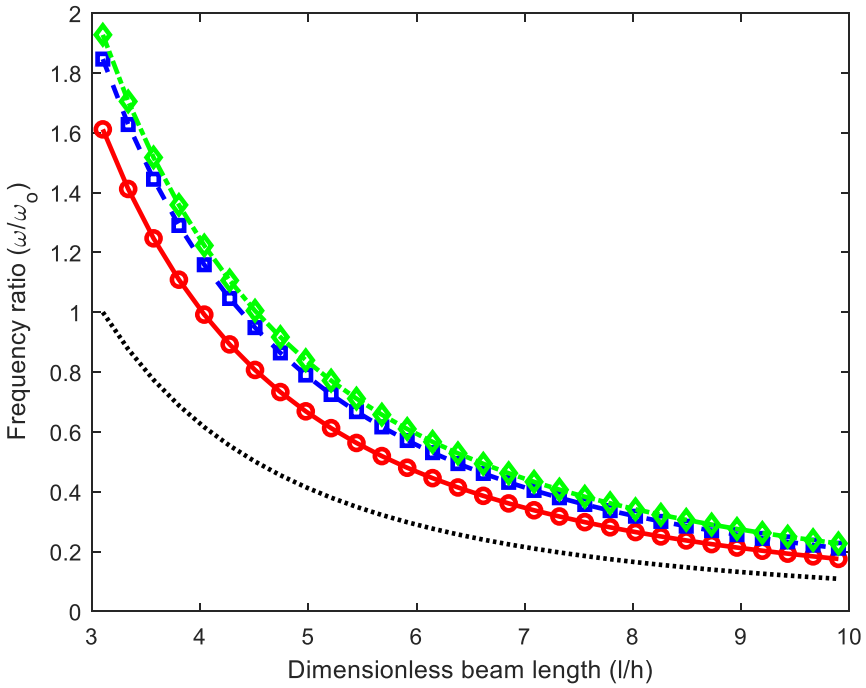

(b)

Fig.2. Effect of CNTs on fundamental frequency of CNTs-reinforced FG composite beams. (a) V_c=1.5% and (b) V_c=5.0% (ω_o is the fundamental frequency of the beam with no CNTs at beam length l=3.1h).

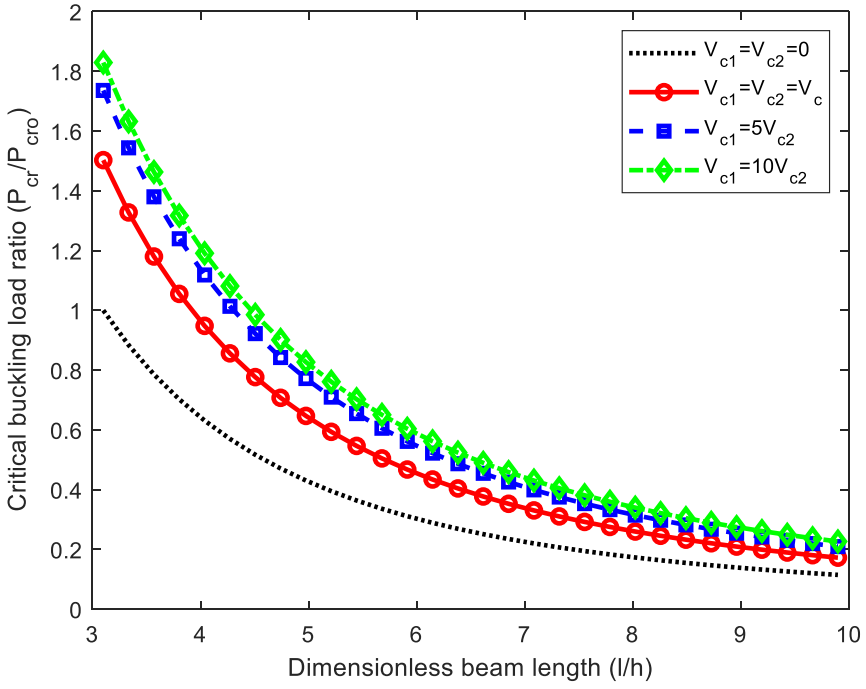

(a)

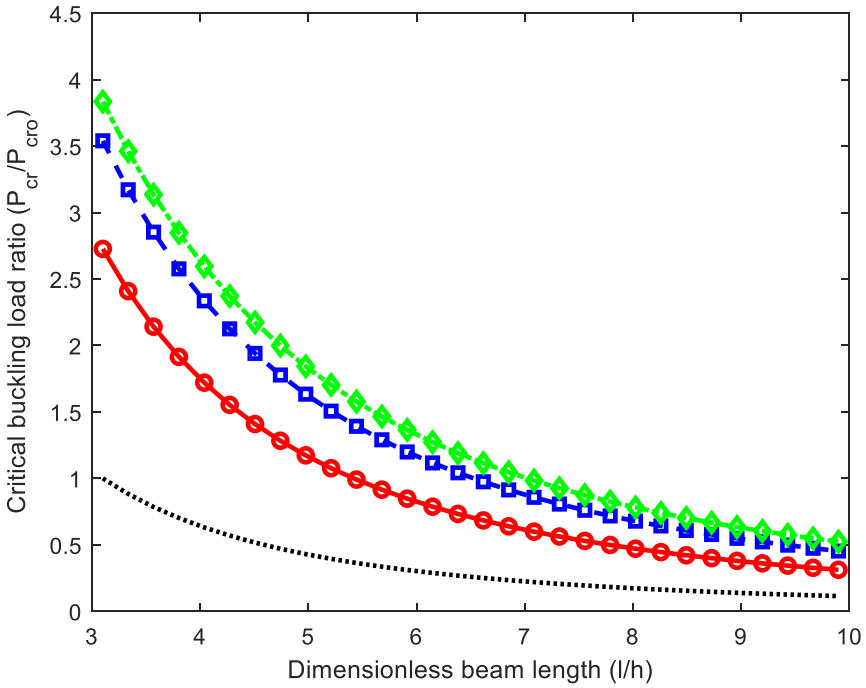

(b)

Fig.3. Effect of CNTs on critical buckling load of CNT-reinforced FG composite beams. (a) V_c=1.5% and (b) V_c=5.0% (P_{cro} is the critical buckling load of the beam with no CNTs at beam length l=3.1h).

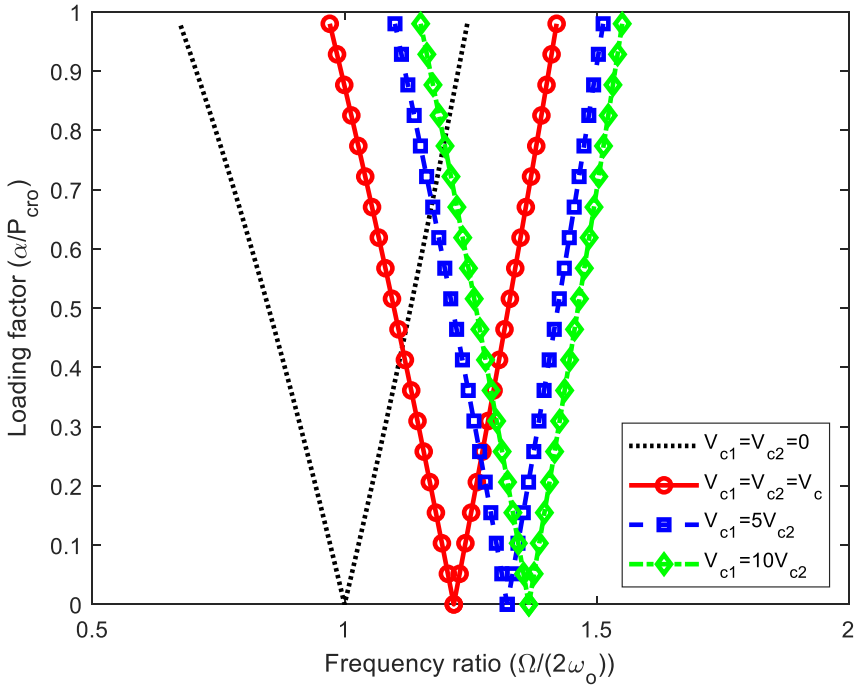

(a)

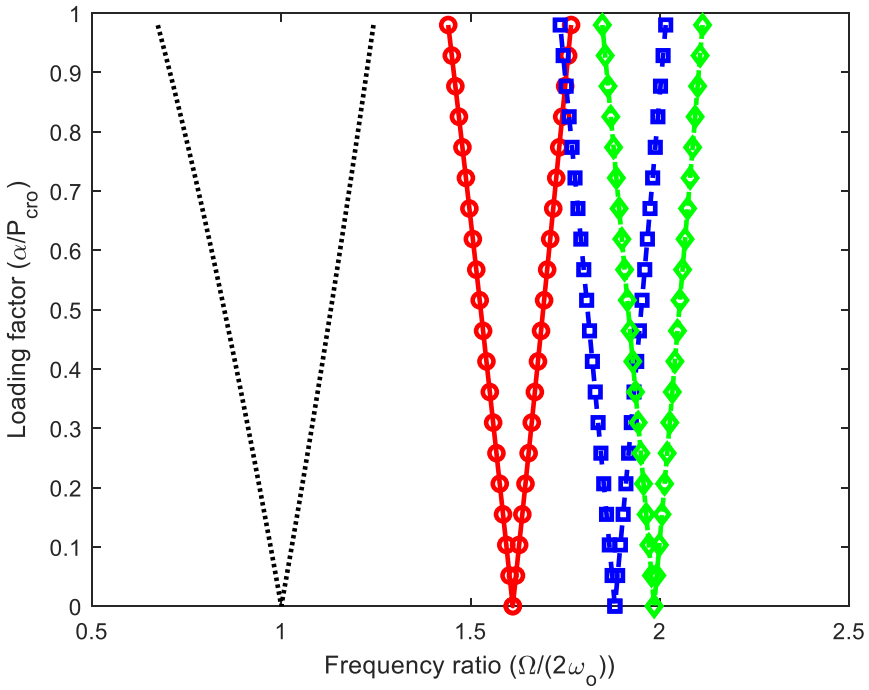

(b)

Fig.4. The dynamic instability zones of CNTs-reinforced FG composite beams. (a) V_c=1.5% and (b) V_c=5.0% (l=4h, ω_o and P_{cro} are the fundamental frequency and critical buckling load of the beam with no CNTs).

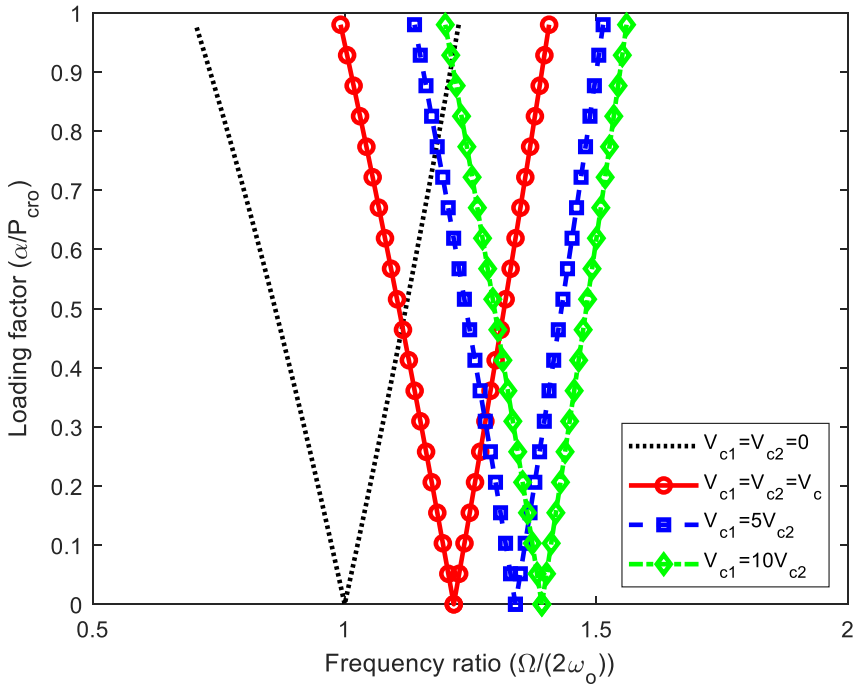

(a)

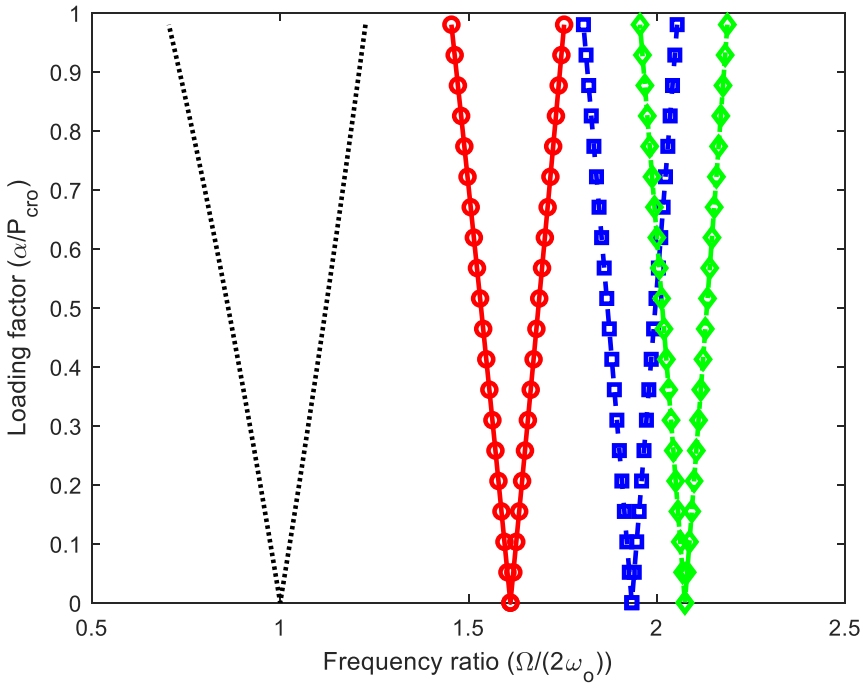

(b)

Fig.5 The dynamic instability zones of CNTs-reinforced FG composite beams. (a) V_c=1.5% and (b) V_c=5.0% (l=8h, ω_o and P_{cro} are the fundamental frequency and critical buckling load of the beam with no CNTs).

Fig.3 shows the variation of the critical buckling load of the composite beams with the beam length for the two different overall volume fractions of CNTs. The results are obtained from the calculation of Eq.(29). Similar to the frequency results, the critical loads of the three composite beams are much greater than that of the reference beam, indicating that the use of CNTs can significantly increase the buckling resistance of the composite beam. The critical loads of the two I-shape CNTs-reinforced FG composite beams are found to be higher than that of the uniformly reinforced CNTs-polymer composite beam, indicating that the use of I-shape FG distribution is more effective in improving the buckling resistance of the beam. The difference in critical load between the two I-shape CNTs-reinforced FG composite beams is also found to be insignificant, indicating that the similar limitation exists if purely increasing the volume fraction of CNTs in the two outer layers of the beams. Finally, the comparison of critical loads shown in Fig.2a and Fig.2b illustrates that, the more CNTs used in the composite beam, the higher the critical load of the beam can be achieved.

The dynamic instability of a structure occurs because of parametric resonance. The dynamic instability zones of a structure thus can be plotted based on the amplitude and excitation frequency of the externally applied dynamic load. Figs.4 and 5 show the dynamic instability zones of the composite beams at two different beam lengths (l/h=4 and l/h=8), each with two different overall volume fractions of CNTs (V_c=1.5% and V_c=5.0%,). The results are obtained from the calculation of Eq.(32).

It can be seen from Fig.4a that the dynamic instability zones of the three composite beams are all smaller than that of the reference beam and they all move, to some extent, towards to high frequency side, indicating that the use of small quantity of CNTs can significantly improve the

dynamic stability of the composite beams. The dynamic instability zones of the two I-shape CNTs-reinforced FG composite beams are found to be moderately smaller than that of the uniformly reinforced CNTs-polymer composite beam and they also further move towards to high frequency side than the uniformly reinforced CNTs-polymer composite beam, indicating that the use of I-shape FG distribution is more effective in reducing the size of instability zone of the beam. The dynamic instability zones of the two I-shape CNTs-reinforced FG composite beams are found to be very similar, except that one with larger CNTs volume fraction in the two outer layers of the beam is shifted a little to the high frequency side. With the increase of the overall volume fractions of CNTs to V_c=5.0% (see Fig.4b), the difference between the four dynamic instability zones also growths, although their qualitative features remain unchanged. From the comparison of the results between Fig.4 and Fig.5, one can see the dynamic instability zones shown in the two figures are very similar although they have different beam lengths. The reason for that is because both the amplitude and excitation frequency of the dynamic load plotted in the figures have been normalized by using the fundamental frequency and critical buckling load of the beam with no CNTs, which eliminate the main effect of the beam length.

The dynamic instability charts plotted in Figs.4 and 5 provide important information on the resonance of the FG composite beams. The charts illuminate the interaction between the amplitude and frequency of the axial excitation loading and describe how the resonance of the beams changes with them. The figures also show how to functionally grade the composite beams which can effectively reduce the resonance potential of the composite beams. In recent years FG composite materials have been widely used as the structural components to make sensors and biomedical implants. It is therefore very important to understand the dynamic behavior and instability feature of the components made by FG composite materials when they are working in a dynamic environment.

5. Conclusions

This paper has proposed a I-type CNTs-reinforced FG composite beams. By using Halpin–Tsai model the section properties of the FG composite beams have been assessed and the analyses of the free vibration, buckling and dynamic instability of the FG composite beams when subjected to axial excitation loading have also been carried out. Analytical expressions of determining the free vibration frequency, critical buckling load, and excitation frequency of resonance of the FG composite beams have been derived. From the results obtained the following conclusions can be drawn:

(1) The use of CNTs to reinforce and/or functionally grade polymer beam can significantly increase its frequency of transverse vibration and axially compressive buckling load and improve its dynamic stability when the beam is subjected to axial excitation loading. The more the CNTs are used in the beam the more improvement can be achieved.
(2) It is more effective and more efficient to use I-shape distribution of CNTs to functionally grade the beam than the traditional use of uniform distribution of CNTs on the cross-section of the beam. It is demonstrated that both the fundamental frequency and critical buckling load of the I-shape distributed CNTs-reinforced FG composite beam are greater than those of the uniformly distributed CNTs reinforced FG composite beam.
(3) The width of the dynamic instability zone of the I-shape CNTs-reinforced FG composite beam is smaller than that of the uniformly reinforced CNTs-polymer composite beam and corresponding zone position also shifts towards to high frequency side. However, no significant difference in their dynamic instability zones is found between the two I-shape CNTs reinforced FG composite beams.

(4) The improvement of CNTs reinforcement on the dynamic stability of composite beams will be different for beams of different lengths. However, when the dynamic instability zone is plotted using dimensionless frequency and dimensionless loading amplitude the main influence of the beam length on the plotted dynamic instability zone could be eliminated.
(5) The resonance characteristics of the CNTs-reinforced FG composite beams can be significantly improved by the use of I-shape distribution of CNTs on the beam cross-section, which is demonstrated by not only the reduction of the width of the instability zone but also the shift of the instability zone from the low frequency side to the high frequency side.

Acknowledgments – The work presented in the paper was supported by the Korean Agency for Infrastructure Technology Advancement (KAIA) via a research grant funded to the University of Plymouth by the Ministry of Land, Infrastructure and Transport (21CTAP-C151808-03), South Korea.

Declaration of interests - The authors declare that they have no known competing financial interests or personal relationships that could have appeared to influence the work reported in this paper.

References

[1] M. Paradise, T. Goswami, Carbon nanotubes – production and industrial applications, Materials & Design 28(5) (2007) 1477-1489.
[2] I. Kang, Y.Y. Heung, J.H. Kim, J.W. Lee, R. Gollapudi, S. Subramaniam, S. Narasimhadevara, D. Hurd, G.R. Kirikera, V. Shanov, M.J. Schulz, D. Shi, J. Boerio, S. Mall, M. Ruggles-Wren, Introduction to carbon nanotube and nanofiber smart materials, Composites Part B: Engineering 37(6) (2006) 382-394.
[3] A.M. El-Ashmawy, Y.M. Xu, L.A. El-Mahdy, Mechanical properties improvement of bi-directional functionally graded laminated MWCNT reinforced composite beams using an integrated tailoring–optimization approach, Microporous and Mesoporous Materials 314 (2021) 110875.
[4] J.N. Coleman, U. Khan, W.J. Blau, Y.K. Gun'ko, Small but strong: A review of the mechanical properties of carbon nanotube–polymer composites, Carbon 44 (2006) 1624–1652.
[5] A. Chakraborty, S. Gopalakrishnan, J. Reddy, A new beam finite element for the analysis of functionally graded materials, Int. J. Mech. Sci. 45(3) (2003) 519–539.
[6] X.-F. Li, A unified approach for analyzing static and dynamic behaviors of functionally graded Timoshenko and Euler–Bernoulli beams, J. Sound Vib. 318(4–5) (2008) 1210–1229.
[7] M. Şimşek, Static analysis of a functionally graded beam under a uniformly distributed load by Ritz method, Int. J. Eng. Appl. Sci. 1(3) (2009) 1–11.
[8] Y. Huang, X.-F. Li, A new approach for free vibration of axially functionally graded beams with non-uniform cross-section, J. Sound Vib. 329(11) (2010) 2291–2303.
[9] A.E. Alshorbagy, M. Eltaher, F. Mahmoud, Free vibration characteristics of a functionally graded beam by finite element method, Appl. Math. Model. 35(1) (2011) 412–425.
[10] M. Lezgy-Nazargah, M. Shariyat, S. Beheshti-Aval, A refined high-order globallocal theory for finite element bending and vibration analyses of laminated composite beams, Acta Mech. 217(3–4) (2011) 219–242.

[11] H. Rokni, A.S. Milani, R.J. Seethaler, Maximum natural frequencies of polymer composite micro-beams by optimum distribution of carbon nanotubes, Mater. Des. 32(6) (2011) 3389–3398.
[12] H. Rokni, A.S. Milani, R.J. Seethaler, K. Stoeffler, Improvement in dynamic properties of laminated MWCNT-polystyrene composite beams via an integrated numerical–experimental approach, Compos. Struct. 94(8) (2012) 2538–2547.
[13] R. Ansari, M.F. Shojaei, V. Mohammadi, R. Gholami, F. Sadeghi, Nonlinear forced vibration analysis of functionally graded carbon nanotube-reinforced composite Timoshenko beams, Compos. Struct. 113 (2014) 316–327.
[14] M. Filippi, E. Carrera, A. Zenkour, Static analyses of FGM beams by various theories and finite elements, Composites B 72 (2015) 1–9.
[15] M. Lezgy-Nazargah, Fully coupled thermo-mechanical analysis of bi-directional FGM beams using NURBS isogeometric finite element approach, Aerosp. Sci. Technol. 45 (2015) 154–164.
[16] A. El-Ashmawy, M. Kamel, M.A. Elshafei, Thermo-mechanical analysis of axially and transversally Function Graded Beam, Composites B 102 (2016) 134–149.
[17] N. Shafiei, M. Kazemi, Buckling analysis on the bi-dimensional functionally graded porous tapered nano-/micro-scale beams, Aerosp. Sci. Technol. 66 (2017) 1–11.
[18] T. Yang, Y. Tang, Q. Li, X.-D. Yang, Nonlinear bending, buckling and vibration of bi-directional functionally graded nanobeams, Compos. Struct. 204 (2018) 313–319.
[19] A. Lal, K. Markad, Deflection and stress behaviour of multi-walled carbon nanotube reinforced laminated composite beams, Comput. Concr. 22(6) (2018) 501–514.
[20] M. Ranjbar, S. Feli, Low velocity impact analysis of an axially functionally graded carbon nanotube reinforced cantilever beam, Polym. Compos. 39(S2) (2018) E969–E983.
[21] S. Zheng, D. Chen, H. Wang, Size dependent nonlinear free vibration of axially functionally graded tapered microbeams using finite element method, Thin-Walled Struct. 139 (2019) 46–52.
[22] M.J. Aubad, S.O.W. Khafaji, M.T. Hussein, M.A. Al-Shujairi, Modal analysis and transient response of axially functionally graded (AFG) beam using finite element method, Mater. Res. Express 6(10) (2019) 1065g4.
[23] S. Sahmani, B. Safaei, Nonlinear free vibrations of bi-directional functionally graded micro/nano-beams including nonlocal stress and microstructural strain gradient size effects, Thin-Walled Struct. 140 (2019) 342–356.
[24] Y. Tang, X. Lv, T. Yang, Bi-directional functionally graded beams: asymmetric modes and nonlinear free vibration, Composites B 156 (2019) 319–331.
[25] M. Heidari, H. Arvin, Nonlinear free vibration analysis of functionally graded rotating composite Timoshenko beams reinforced by carbon nanotubes, J. Vib. Control 25(14) (2019) 2063–2078.
[26] X. Chen, X. Zhang, Y. Lu, Y. Li, Static and dynamic analysis of the postbuckling of bi-directional functionally graded material microbeams, Int. J. Mech. Sci. 151 (2019) 424–443.
[27] A. Lal, K. Markad, Thermo-mechanical post buckling analysis of multiwall carbon nanotube-reinforced composite laminated beam under elastic foundation, Curved Layer. Struct. 6(1) (2019) 212–228.
[28] S. Sahmani, B. Safaei, Influence of homogenization models on size-dependent nonlinear bending and postbuckling of bi-directional functionally graded micro/nano-beams, Appl. Math. Model. 82 (2020) 336–358.
[29] F. Bourada, A.A. Bousahla, A. Tounsi, E. Bedia, S. Mahmoud, K.H. Benrahou, A. Tounsi, Stability and dynamic analyses of SW-CNT reinforced concrete beam resting on elastic-foundation, Comput. Concr. 25(6) (2020) 485–495.

[30] A. El-Ashmawy, Y. Xu, Longitudinal modeling and properties tailoring of functionally graded carbon nanotube reinforced composite beams: A novel approach, Appl. Math. Model. 88 (2020) 161–174.
[31] J. Yang, X.H. Huang, H.S. Shen, Nonlinear flexural behavior of temperature dependent FG-CNTRC laminated beams with negative Poisson's ratio resting on the Pasternak foundation, Eng. Struct. 207 (2020) 110250.
[32] H.B. Khaniki, M.H. Ghayesh, On the dynamics of axially functionally graded CNT strengthened deformable beams, Eur. Phys. J. Plus 135(6) (2020) 415.
[33] F. Hou, S. Wu, Z. Moradi, N. Shafiei, The computational modeling for the static analysis of axially functionally graded micro-cylindrical imperfect beam applying the computer simulation, Engineering with Computers (2021) (online published, https://doi.org/10.1007/s00366-021-01456-x)
[34] A. Shariati, D. Jung, H. Mohammad-Sedighi, K.K. Żur, M. Habibi, M. Safa, Stability and dynamics of viscoelastic moving Rayleigh beams with an asymmetrical distribution of material parameters, Symmetry 12(4) (2020) 586.
[35] F. Ebrahimi, D. Hashemabadi, M. Habibi, H. Safarpour, Thermal buckling and forced vibration characteristics of a porous GNP reinforced nanocomposite cylindrical shell, Microsystem Technologies 26 (2020) 461–473.
[36] H. Moayedi, M. Habibi, H. Safarpour, M. Safarpour, L. K. Foong, Buckling and frequency responses of a gaphene nanoplatelet reinforced composite microdisk, International Journal of Applied Mechanics 11(10) (2019) 1950102.
[37] M. Fouaidi, M. Jamal, A. Zaite, N. Belouaggadia, Bending analysis of functionally graded graphene oxide powder-reinforced composite beams using a meshfree method, Aerospace Science and Technology 110 (2021) 106479.
[38] H.B. Khaniki, M.H. Ghayesh, A review on the mechanics of carbon nanotubes strengthened deformable structures, Engineering Structures 220 (2020) 110711.
[39] V.V. Bolotin, The Dynamic Stability of Elastic Systems, 1964, San Francisco, CA, Holden-day, Inc.
[40] J.S. Huang, L. H. Hung, Dynamic stability for a simply supported beam under periodic axial excitation, Int. J. of Nonliner Mech. 19(4) (1984) 287-301.
[41] J. Zhu, S.G. Qian, L.Y. Li, Dynamic instability of laterally-restrained zed-purlin beams under uplift loading, International Journal of Mechanical Sciences 131-132 (2017) 408-413.
[42] J.S. Lei, B. Kim, L.Y. Li, Dynamic Instability Analysis of Axially Compressed Castellated Columns, International Journal of Steel Structures 20(2) (2020) 559-566.
[43] J. Zhu, S.G. Qian, L.Y. Li, Dynamic instability of channel-section beams under periodic loading, Mechanics of Advanced Materials and Structures 27(10) (2020) 840-849.
[44] J.C. Halpin, J.L. Kardos, The Halpin–Tsai equations: a review, Polym Eng Sci. 16(5) (1976) 344–52.
[45] M.H. Ghayesh, S. Balar, Non-linear parametric vibration and stability analysis for two dynamic models of axially moving Timoshenko beams, Applied Mathematical Modelling 34(10) (2020) 2850-2859.
[46] Y. Fang, L.Y. Li, S.H. Jang, Piezoresistive modelling of CNTs reinforced composites under mechanical loadings, Compos. Sci. and Tech. 208 (2021) 108757.
[47] Y. Fang, L.Y. Li, S.H. Jang, Calculation of electrical conductivity of self-sensing carbon nanotube composites, Composites B 199 (2020) 108314.